CHAPTER 13

ANALYSIS OF INDIVIDUAL DEEP FOUNDATIONS UNDER AXIAL LOADING USING THE *t-z* MODEL

13.1 SHORT-TERM SETTLEMENT AND UPLIFT

13.1.1 Settlement and Uplift Movements

Two analytical methods are used to compute the load-settlement curve of an axially loaded pile. One method uses the theory of elasticity. The theories discussed by D'Appolonia and Romualdi (1963), Thurman and D'Appolonia (1965), Poulos and Davis (1968), Poulos and Mattes (1969), Mattes and Poulos (1969), and Poulos and Davis (1980) use methods based on the theory of elasticity. These methods use Mindlin's (1936) equations for stress and deformations at any point in the interior of semi-infinite, elastic, and isotropic solids resulting from a force applied at another point in the solids.

The displacement of the pile is calculated by superimposing the influences of the load transfer in side resistance along the length of the pile and in end bearing at the pile tip. The compatibility of those forces and the displacement of the pile are obtained by solving a set of simultaneous equations. This method takes the stress distribution within the soil into consideration; therefore, the elasticity method presents the possibility of solving for the behavior of a group of closely spaced piles under axial loadings (Poulos, 1968; Poulos and Davis, 1980).

The drawback of the elasticity method lies in the basic assumptions that must be made. The actual ground conditions rarely if ever satisfy the basic assumption of uniform and isotropic material. In spite of the highly nonlinear stress-strain characteristics of soils, the only soil properties considered in the elasticity method are Young's modulus E and the Poisson's ratio v. The use of only two constants, E and v, to represent soil characteristics is too much

of an oversimplification to allow the elasticity-based methods to work in conditions involving stratified soils with differing strengths and compressibilities.

The other method used to calculate the load-settlement curve for an axially loaded pile may be called the *load-transfer method* (commonly referred to as the t-z method). Finite-difference equations are employed to achieve compatibility between pile displacement and the load transfer along a pile and between displacement and resistance at the tip of the pile. This method was first used by Seed and Reese (1957); other studies have been reported by Coyle and Reese (1966), Coyle and Sulaiman (1967), and Kraft et al. (1981). The t-z difference method assumes the Winkler concept; that is, the load transfer at a certain pile section and the pile tip resistance are independent of the pile displacement elsewhere. The close agreement between the prediction and the loading test results in clays (Coyle and Reese, 1966) and the scattering of prediction values for the loading test in sands (Coyle and Sulaiman, 1967) may possibly be explained by the relative sensitivity of a soil to changes in patterns of stress. Admitting the deficiency in the displacement-shear force criteria of sand, the finite-difference method is still practical and potential because it can deal with any complex composition of soil layers with any nonlinear relationship of displacement versus shear force. Furthermore, the method can accommodate improvements in soil criteria with no modifications of the basic theory.

In the following sections, the derivation of the finite-difference equations is shown. The fundamental technique employed here is the same as that used in previous investigations. The difference lies in the computation procedure. The method shown here gives a solution first for the pile displacement at all stations. Then the pile force at each station is calculated. Convergence of the iterative computation is quite fast even near the ultimate load.

13.1.2 Basic Equations

The mechanical model for an axially loaded pile is presented in Figure 13.1. The pile head is subjected to an axial force P_t and undergoes a displacement z_t. The pile-tip displacement is z_{tip}, and the pile displacement at the depth x is z. Displacement z is positive downward, and the compressive force P is positive.

In an element dx (Figure 13.1a), the strain in the element due to the axial force P is calculated by neglecting the second-order term dP.

$$\frac{dz}{dx} = -\frac{P}{EA} \tag{13.1a}$$

or

$$P = -EA\,\frac{dz}{dx} \tag{13.1b}$$

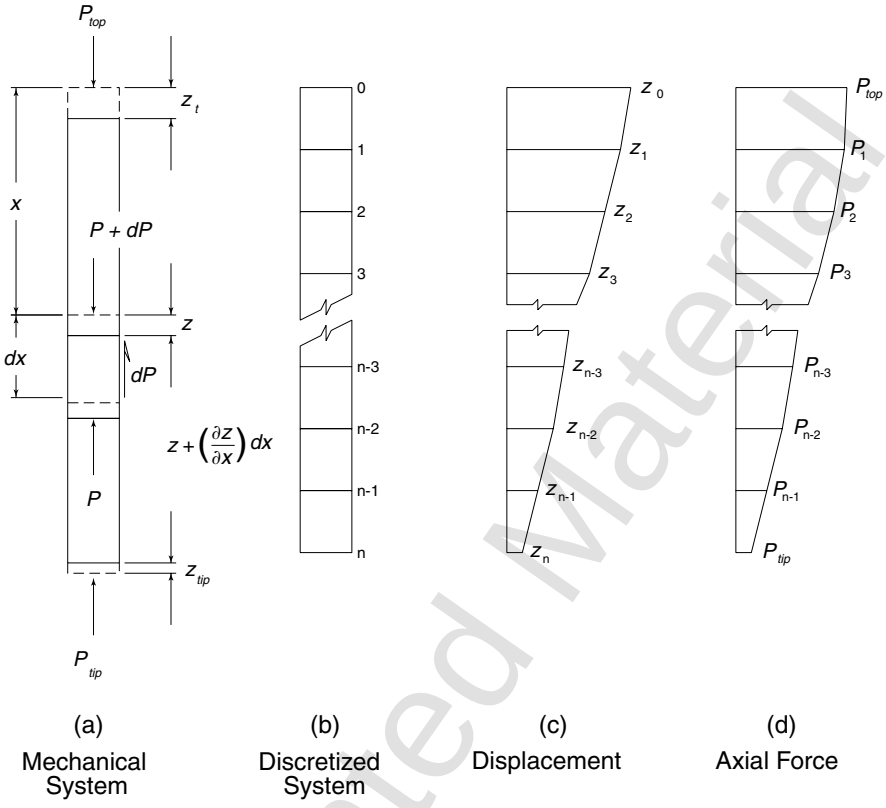

Figure 13.1 Numerical model of an axially loaded pile.

where

P = axial force in the pile in pounds (downward positive),
E = Young's modulus of pile material in psi, and
A = cross-sectional area of the pile in square inches.

The total load transfer through an element dx is expressed by using the modulus μ in the load transfer curve (Figure 13.2a).

$$dP = -\mu\, z\, \ell\, dx \tag{13.2}$$

or

$$\frac{dP}{dx} = -\mu\, z\, \ell \tag{13.3}$$

where

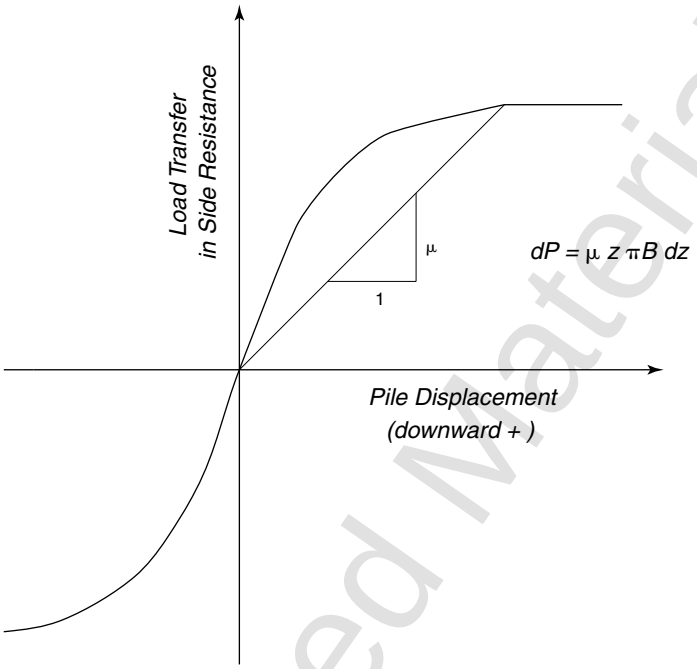

(a) Load Transfer Curve for Side Resistance

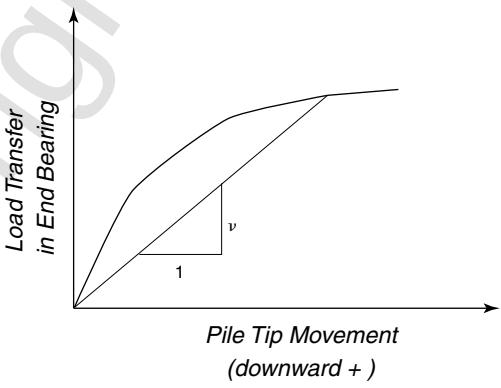

(b) Load Transfer Curve in End Bearing

Figure 13.2 Load-transfer curves for side and tip resistance.

ℓ = circumference of a cylindrical pile or the perimeter encompassing an H-pile, and

μ = modulus in the load transfer curve in Figure 13.2a.

Equation 13.1 is differentiated with respect to x and equated with Eq. 13.3 to obtain Eq. 13.4:

$$\frac{d}{dx} EA \frac{dz}{dx} = \mu z \ell \tag{13.4}$$

The pile-tip resistance is the product of a secant modulus v and the pile-tip movement z_{tip}. (See the curves of pile-tip movement versus resistance, Figure 13.2b).

$$P_{tip} = v z_{tip} \tag{13.5}$$

Equation 13.4 is the basic differential equation that must be solved. Boundary conditions at the tip and at the top of the pile must be established. The boundary condition at the tip of the pile is given by Eq. 13.5. At the top of the pile, the boundary condition may be either a force or a displacement. Treatment of these two cases is presented later.

13.1.3 Finite Difference Equations

Equation 13.6 gives in difference-equation form the differential equation (Eq. 13.4) for solving the axial pile displacement at discrete stations.

$$a_i z_{i+1} + b_i z_i + c_i z_{i-1} = 0 \tag{13.6}$$

for

$$a_i = \tfrac{1}{4} EA_{i+1} + EA_i - \tfrac{1}{4} EA_{i-1} \tag{13.7}$$

$$b_i = -\mu l h^2 - 2EA_i \tag{13.8}$$

$$c_i = -\tfrac{1}{4} EA_{i+1} + EA_i + \tfrac{1}{4} EA_{i-1} \tag{13.9}$$

and where h = increment length or dx.

13.1.4 Load-Transfer Curves

The acquisition of load-transfer curves from a load test requires that the pile be instrumental internally for the measurement of axial load with depth. The number of such experiments is relatively small, and in some cases the data

are barely adequate; therefore, the amount of information that can be used to develop analytical expressions is limited.

Undoubtedly, additional studies will be reported in technical literature from time to time. Any improvements made in load-transfer curves can be readily incorporated into the analyses.

13.1.5 Load-Transfer Curves for Side Resistance in Cohesive Soil

Coyle and Reese (1966) examined the results from three instrumented field tests and the results from rod tests in the laboratory and developed a recommendation for a load-transfer curve. The curve was tested by using results of full-scale experiments with uninstrumented piles. The comparisons of computed load-settlement curves with those from experiments showed agreement that was excellent to fair. Table 13.1 presents the fundamental curve developed by Coyle and Reese.

This table shows that the movement to develop full load transfer is quite small. Furthermore, the curve is independent of soil properties and pile diameter.

Reese and O'Neill (1988) studied of the results of several field-load tests of instrumented bored piles and developed the curves shown in Figure 13.3. This figure shows that the maximum load transfer occurred at approximately 0.6% of the diameter of a pile. Because the piles tested had diameters of 24 to 36 in., the movement at full load transfer would be on the order of 0.2 in., a much larger value than was obtained by Coyle and Reese.

Kraft et al. (1981) studied the theory of load transfer in side resistance and noted that pile diameter, axial pile stiffness, pile length, and distribution of soil strength and stiffness along the pile are all factors that influence load-transfer curves. Equations for computing the curves were presented. Vijayvergiya (1977) also presented a method for obtaining load-transfer curves.

TABLE 13.1 Load Transfer versus Pile Movement for Cohesive Soil

Ratio of Load Transfer to Maximum Load Transfer	Pile Movement, in.
0	0
0.18	0.01
0.38	0.02
0.79	0.04
0.97	0.06
1.00	0.08
0.97	0.12
0.93	0.16
0.93	0.20

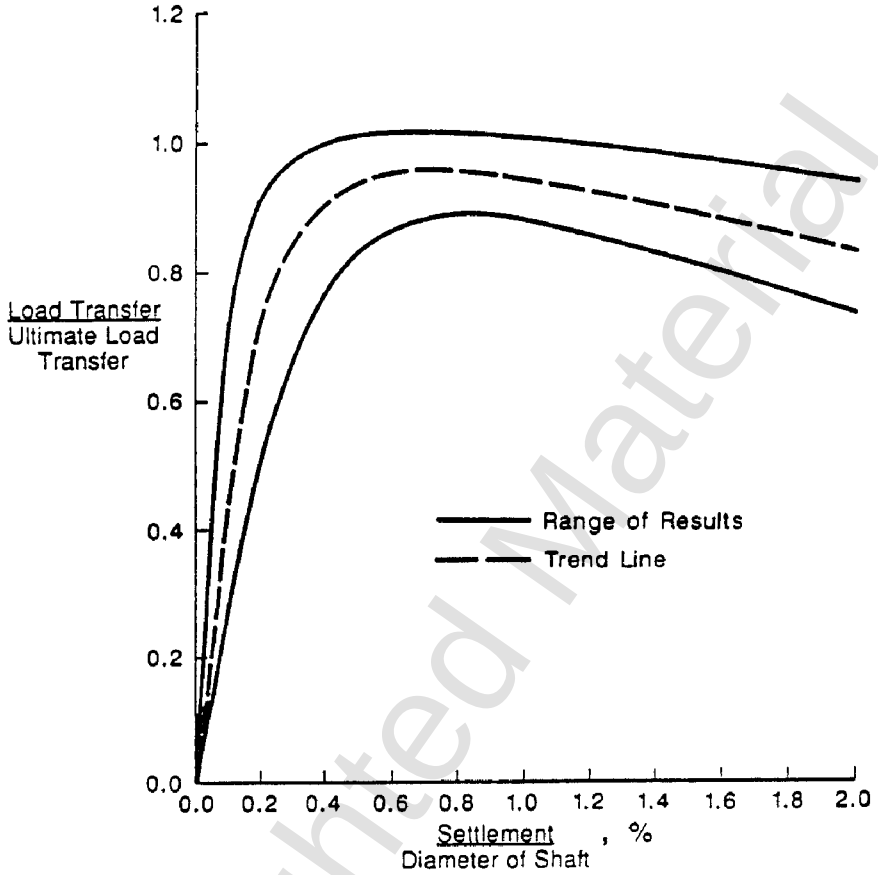

Figure 13.3 Normalized curves showing load transfer in side resistance versus settlement for drilled shafts in clay (after Reese and O'Neill, 1988).

The details of the methods of Kraft et al. and Vijayvergiya are not presented here.

13.1.6 Load-Transfer Curves for End Bearing in Cohesive Soil

The work of Skempton (1951) (also cited in the discussion of lateral loading) was employed, and a method was developed for predicting the load in end bearing of a pile in clay as a function of the movement of the pile tip. The laboratory stress-strain curve for the clay at the base of the pile was obtained by testing, or was estimated from values given by Skempton for laboratory strain, ε_{50}, at one-half of the ultimate compressive strength of the clay. Skempton reported that ε_{50} ranged from 0.005 to 0.02. He also used the theory of elasticity to develop approximate equations for the settlement of a footing

(base of a pile) using laboratory stress-strain curves. Skempton's equations are as follows:

$$q_b = N_c \frac{\sigma_f}{2} \tag{13.10}$$

$$\frac{w}{B} = 2\varepsilon \tag{13.11}$$

where

q_b = failure stress in bearing at the base of the footing,
σ_f = failure compressive stress in the laboratory unconfined-compression or quick triaxial test,
N_c = bearing capacity factor (Skempton recommended 9.0)
B = diameter of the footing or equivalent length of a side for a square or rectangular shape,
ε = strain measures from the unconfined-compression or quick-triaxial test, and
w_b = settlement of the footing or base of the pile.

Stress-strain curves from a number of laboratory tests have been found to have a slope of approximately 0.5 when plotted on logarithmic scales. Therefore, in the absence of a laboratory stress-strain curve, a parabola can be used to yield a stress-strain curve up to the failure stress. The value of ε_{50} selected will depend on whether the clay is brittle or plastic.

The following is an example of the Skempton relationships. The basic data are:

$$B = 30 \text{ in. } (2.5 \text{ ft})$$

$$c = 780 \text{ psf}$$

$$\varepsilon_{50} = 0.01$$

The basic equation for load versus settlement at the tip of the pile is

$$Q_b = K_b (w_b)^n \tag{13.12}$$

where K_b is a fitting factor. If n is selected as 0.5, K_b can be evaluated as follows:

$$\frac{Q_b}{2} = \frac{N_c c A_{\text{tip}}}{2} = \frac{(9)(780)\pi(1.25)^2}{2} = 17{,}230 \text{ lb}$$

$$w_b = 2\,B\,\varepsilon_{50} = (2)(30 \text{ in.})(0.01) = 0.60 \text{ in.}$$

$$K_b = \frac{Q_b}{w_b^{0.5}} = 22{,}240$$

The curve shown in Table 13.2 can then be computed using Equation 13.12. In this example, it is assumed that the load will not drop as the tip of the pile penetrates the clay.

Reese and O'Neill (1988) studied the results of several tests of bored piles in clay where measurements yielded load in end bearing versus settlement. Figure 13.4 resulted from their studies. A study of the mean curve for the example given above shows that a value of about 1.2 in. is obtained at the ultimate bearing stress rather than the value of 2.4 in. found by the method adapted from Skempton's work. However, the range of values shown by Wright (1977) will easily encompass the earlier result.

Note that the movement of a pile causing the full load transfer in end bearing is several times than that which is necessary to develop full load transfer in skin friction. The above concept is easily demonstrated by considering the soil elements that are strained in end bearing compared to the soil elements that are strained in skin friction.

13.1.7 Load-Transfer Curves for Side Resistance in Cohesionless Soil

Coyle and Sulaiman (1967) studied the load transfer in skin friction of steel piles driven into sand and obtained the curves shown in Figure 13.5. The piles

TABLE 13.2 Load Transfer in Side Resistance for Cohesive Soil

Tip load Q_b, lb	Tip Movement w_b, in.
0	0
2,200	0.01
4,450	0.04
7,000	0.10
12,100	0.30
17,230	0.60
24,500	1.20
34,460	2.40
34,460	10.00

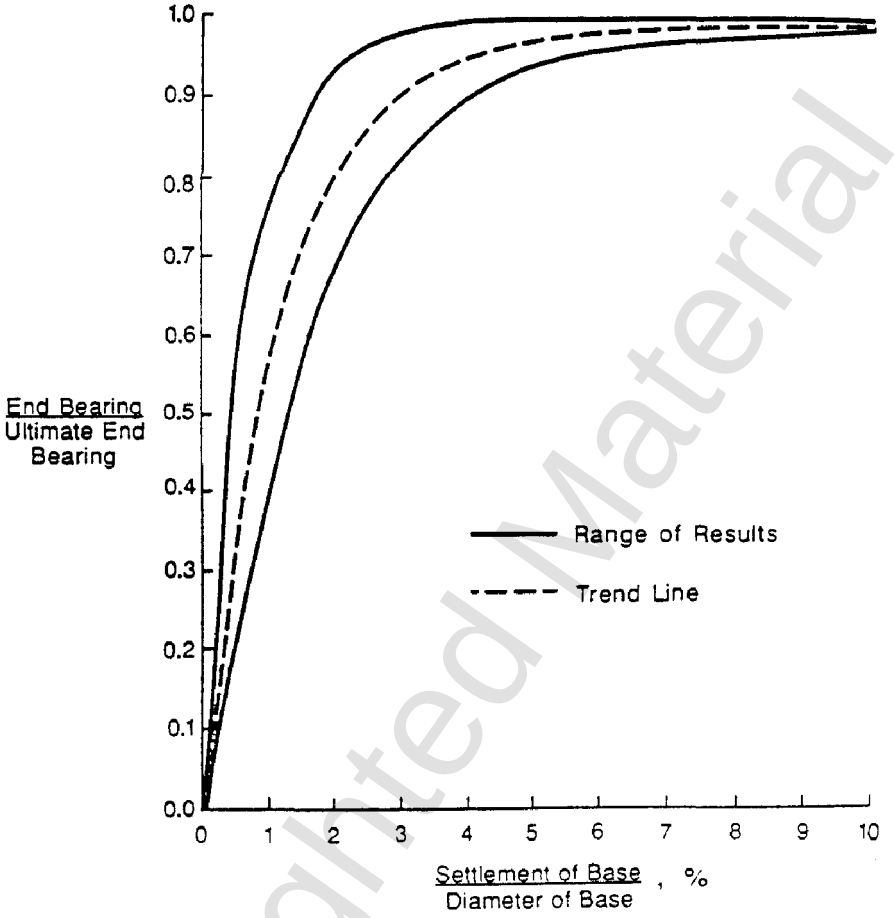

Figure 13.4 Normalized curves showing load transfer in end bearing versus settlement for drilled shafts in clay (after Reese and O'Neill, 1988).

had diameters ranging from 13 to 16 in. and a penetration of about 50 ft. An examination of the shape of the curves showed that they could be fitted with the following equation:

$$f = K_s\left(\frac{w}{B}\right)^{0.15}, \quad \left(\frac{w}{B}\right) \leq 0.07 \tag{13.13}$$

where

f = load transfer in side resistance,
w = movement of pile,

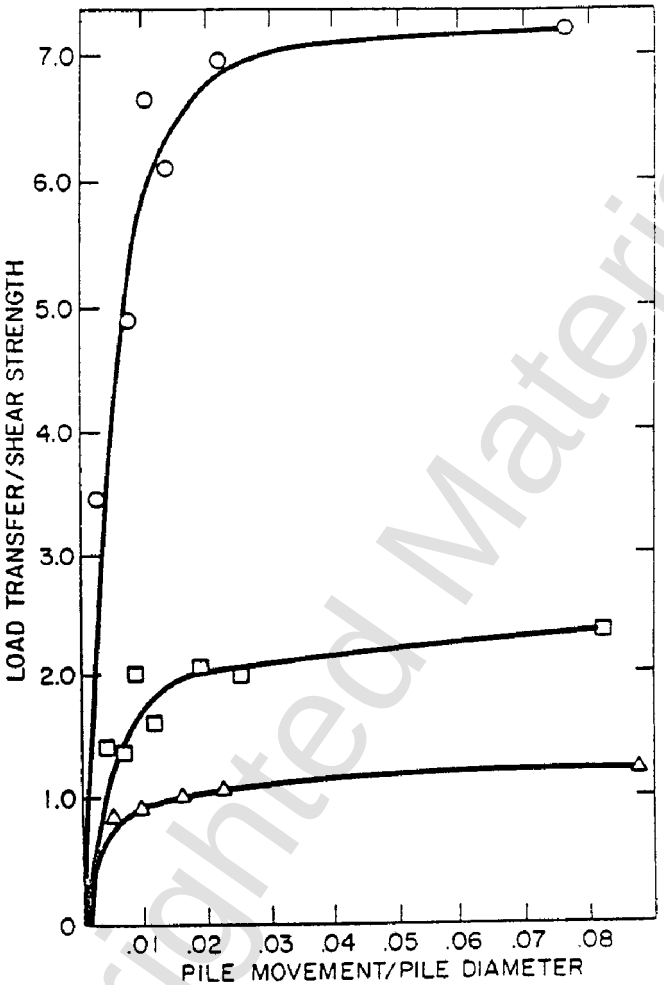

Figure 13.5 Experimental load-transfer curves in side resistance for sand (after Coyle and Sulaiman, 1967).

B = pile diameter, and
K_s = fitting factor.

Equation 13.13 can be used to obtain the approximate load transfer in skin friction for a pile in sand. The value of the maximum unit load transfer $f_{\max}$ would be obtained by use of appropriate equations. The value of the fitting factor K_s can be found by using the following equation:

$$f_{\max} = K_s(0.07)^{0.15} \tag{13.14}$$

The curves are assumed to be flat for movements larger than $0.07B$. While Eq. 13.14 and Figure 13.5 show that the load transfer continues to increase to a movement of $0.07B$, the maximum load transfer essentially occurs at a movement of about $0.03B$.

O'Neill and Reese (1999) examined the results of load tests of a number of full-sized bored piles that were instrumented for the measurement of axial load with respect to depth. The results of this study showed that the curves for cohesionless soils were similar to those for cohesive soils and that Figure 13.6 can be used for cohesionless soils.

Mosher (1984) studied the transfer of load in skin friction (side resistance) of axially loaded piles driven into sand. He developed the following equation and Table 13.3 for obtaining *t-z* (load transfer curves):

$$f = \frac{w}{\dfrac{1}{E_i} + \dfrac{1}{f_{\max}}\, w} \tag{13.15}$$

where

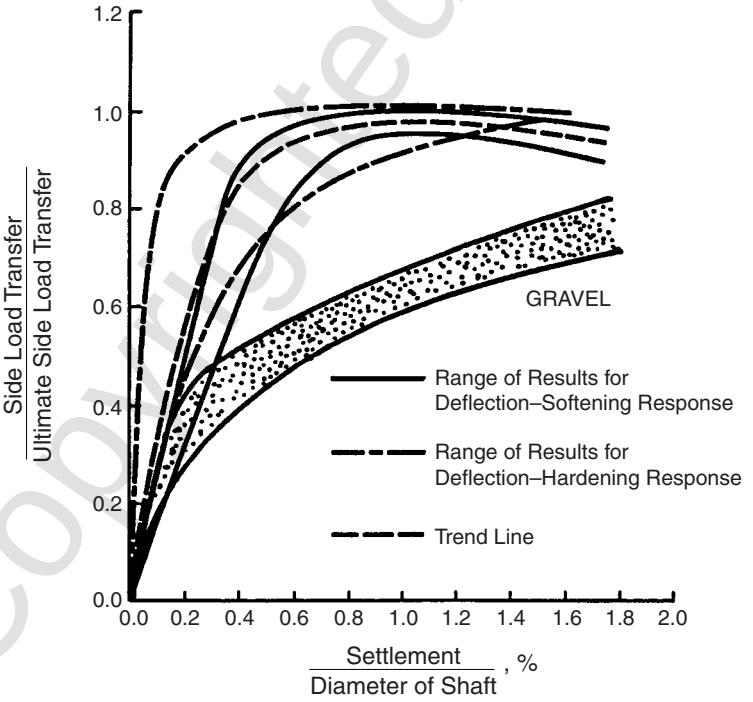

Figure 13.6 Normalized curves showing load transfer in side resistance versus settlement for drilled shafts in cohesionless soil (from O'Neill and Reese, 1999).

TABLE 13.3 Mosher's Values of E_s for Sand for Use in *f*-*w* Curves

Relative Density	ϕ, degrees	E_s, kPa/m	E, lb/ft^2/in.
Loose	28–31	6.3×10^{-2}–10.5×10^{-2}	(6,000–10,000)
Medium	32–34	10.5×10^{-2}–14.7×10^{-2}	(10,000–14,000)
Dense	35–38	14.7×10^{-2}–18.9×10^{-2}	(14,000–18,000)

f = unit load transfer, lb/ft^2
w = pile movement, in.
$f_{\max}$ = maximum unit load transfer, lb/ft^2, and
E_s = soil modulus, lb/ft^2/in.

The mixed dimensions for E_s should be noted and followed when using Eq. 13.15 in design computation.

13.1.8 Load-Transfer Curves for End Bearing in Cohesionless Soil

Vesić (1970) proposed the following equation for computing the load versus tip settlement for piles in sand after studying the literature and performing several careful experiments:

$$w = \frac{C_w Q_p}{(1 + D_r^2)\, B\, q_b} \tag{13.16}$$

where

w = settlement,
Q_p = tip load,
D_r = relative density, decimal,
B = diameter of tip,
q_b = ultimate base resistance, and
C_w = settlement coefficient (the author found the following values: 0.0372 for driven piles, 0.0465 for jacked piles, and 0.167 for buried, or bored, piles).

(Note: Equation 13.16 is not dimensionally homogeneous, so values of C_w were recomputed and are dependent on the system of units being used.)

Reese and O'Neill (1988) studied the results of experiments with drilled shafts and developed Figure 13.7. The information in this figure was developed from a relatively small amount of data and this method, like other methods presented in this chapter, should be used with appropriate discretion.

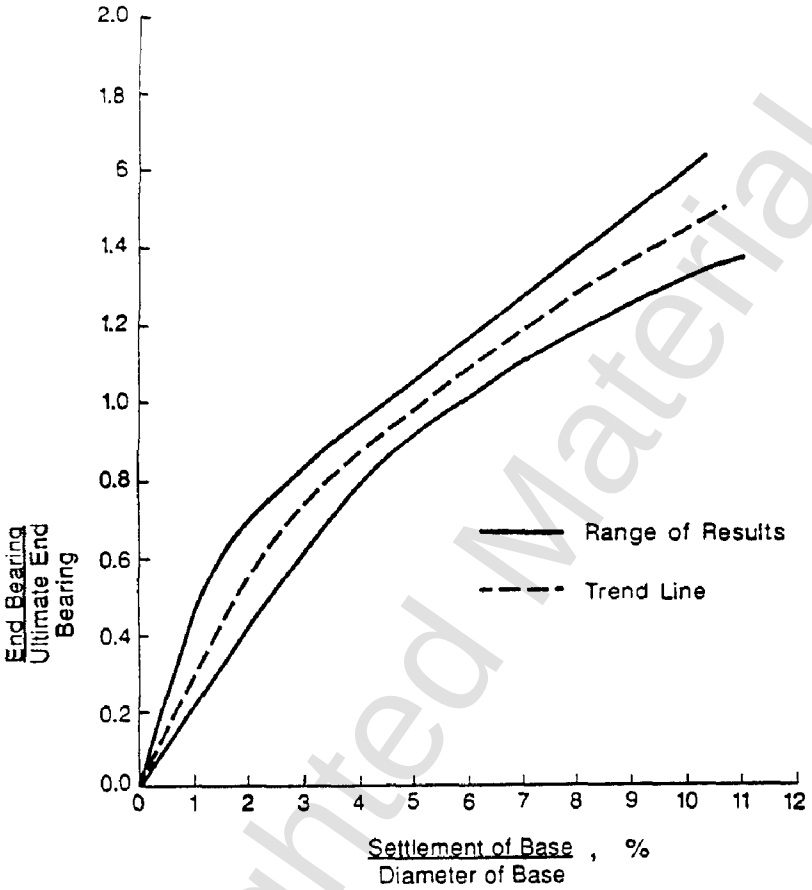

Figure 13.7 Normalized curves showing load transfer in end bearing versus settlement for drilled shafts in cohesionless soil (after Reese and O'Neill, 1988).

13.1.9 Load-Transfer Curves for Cohesionless Intermediate Geomaterials

Load-deformation behavior of drilled shaft sockets in cohensionless intermediate geomaterials can be computed using methods similar to those described for drilled shafts in soft rock. A total load-settlement method, as originally developed by Randolph and Wroth (1978), is recommended.

In the following, only the load-settlement behavior of the socket is described. Elastic shortening in the overburden (generally 0.25–2.0 mm, depending on load and socket depth) will need to be added to the computed settlement to obtain the settlement at the shaft head.

The load-settlement relation for the rock socket is the three-branched curve shown in Figure 13.8. For a given load Q_t at the top of the socket, the cor-

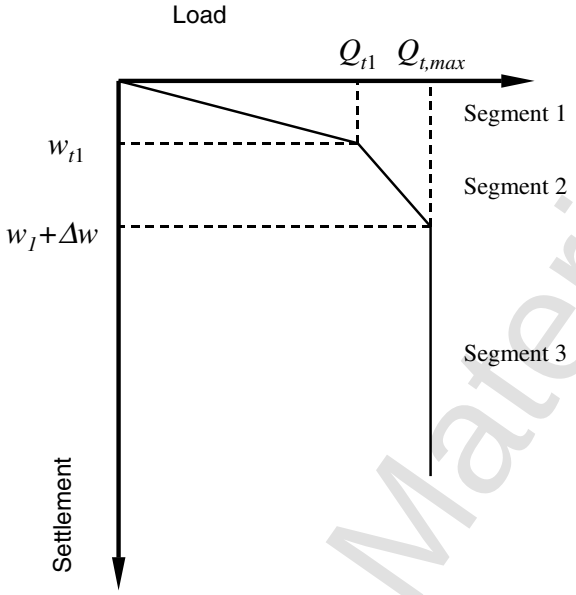

Figure 13.8 Hypothetical load-settlement relationship for the method of Mayne and Harris.

responding elastic settlement along Segment 1, w_t, is computed from Eq. 13.17:

$$w_t = \frac{Q_t I}{E_{sL} B} \tag{13.17}$$

Here E_{sL} is Young's modulus of the granular geomaterial along the sides of the socket at the base level (as distinguished from the geomaterial below the base.)

Based on correlations between energy-corrected SPT tests and Young's moduli (E_s) determined from dilatometer testing in Piedmont residuum, Mayne and Harris (1993) suggest

$$E_s = 22 P_a \, N_{60}^{0.82} \tag{13.18}$$

in which N_{60} is the SPT blow count for this condition in which the energy transferred to the top of the drivestring is 60% of the dwp energy of the SPT hammer, P_a, is the atmospheric pressure (101.3 kPa, or 14.7 psi). More accurate estimates of E_s (and K_0) might be possible if field test results obtained from pressuremeter, flat plate dilatometer, or seismic data are available for the project site.

Mayne and Harris provided a closed-form solution for I for straight-sided shafts from the original solution of Randolph and Wroth, given in Eq. 13.19:

$$I = 4(1 + v) \frac{1 + \dfrac{8 \tanh(\mu L)L}{\pi\lambda(1 - v)\xi(\mu L)D}}{\left[\dfrac{4}{(1 - v)\xi}\right] + \left[\dfrac{4\pi \dfrac{E_{sm}}{E_{sL}} \tanh(\mu L)L}{\zeta(\mu L)D}\right]} \tag{13.19}$$

where

v = Poisson's ratio of the geomaterial, which can be taken as approximately 0.3 for gravel unless evidence indicates otherwise.
L = socket length, and
μL = a lateral extent influence factor for elastic settlement, which can be taken to be

$$\mu L = 2\sqrt{\frac{2}{\zeta\lambda}} \left(\frac{L}{D}\right) \tag{13.20}$$

where

$$\zeta = \ln\left|\left\{0.25 + \left[2.5 \frac{E_{sm}}{E_{sL}} (1 - v) - 0.25\right]\xi\right\} \frac{2L}{D}\right| \tag{13.21}$$

$$\lambda = 2(1 + v) \frac{E_c}{E_{sL}} \tag{13.22}$$

E_c = Young's modulus of the composite (steel and concrete) cross section of the drilled shaft, and
E_{sm} = Young's modulus of soil at the mid-depth of the socket.
E_{sL} = Young's modulus of soil at the base of the socket.

Where the decomposed rock becomes stronger with depth (N increases with depth along the socket), E_{sm}/E_{sL} can ordinarily be taken to be 0.5.

$$\xi = \frac{E_{sL}}{E_b}$$

where E_b = Young's modulus of the granular geomaterial beneath the base of the drilled shaft, which can be different from E_{sL}.

In modeling drilled shaft load tests in Piedmont residuum in the Atlanta, Georgia, area, E_b must be taken to be about 0.4 E_{sL} to obtain an optimum match with the measured load-settlement relations. That is, $\xi = 2.5$.

A schematic of the variation of soil moduli for this method is shown in Figure 13.9.

Equation 13.17 is used to model load versus settlement only until the maximum side resistance, $Q_{s\,\max}$, has been reached (segment 1, Figure 13.8).

$$Q_{s,\max} = f_{\max}\ \pi DL \tag{13.23}$$

and

$$Q_t \text{ (end of segment 1)} = Q_{t1}$$

$$Q_{t1} = \frac{Q_{s,\max}}{1 - \left\{\dfrac{I}{[\xi \cosh(\mu L)][(1 - v)(1 + v)]}\right\}} \tag{13.24}$$

Equation 13.24 is valid approximately for $\xi < 20$. The settlement at the top of the socket at the end of segment 1, w_{t1}, can be determined by letting $Q_t = Q_{t1}$, in Eq. 13.17.

Equations 13.17 and 13.24 define the end of linear segment 1 and the beginning of linear segment 2. At this point, the load on the base at the end of segment 1 is

$$Q_{b1} = Q_{t1} - Q_{s\ \max}.$$

The load at the end of segment 2 is the maximum total resistance of the shaft in the given gravel:

$$Q_{t,\max} = Q_{s,\ \max} + Q_{b,\ \max}.$$

If the side resistance is perfectly plastic (no load softening or hardening after a movement of w_{t1}), then

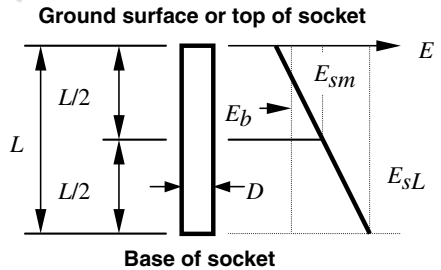

Figure 13.9 Potential soil modulus for computing settlement in granular decomposed rock.

$$Q_{t,\max} = f_{\max}(\pi DL) + q_{\max}\left(\frac{\pi D^2}{4}\right) \tag{13.25}$$

The corresponding settlement at the end of segment 2 is approximately w_{t1} plus the base settlement, Δw_b, due to the increment of base load $Q_{t,\max} - Q_{t1}$, which is given by

$$\Delta w_b = (Q_{t,\max} - Q_{t1})\frac{(1 - v)(1 + \mu)}{E_b D} \tag{13.26}$$

Finally, the end of segment 2 is defined by $Q_{t,\max}$ and $(w_{t1} + \Delta w_b)$. Segment 3 is a line defining continued settlement at no increasing load, which is probably conservative for most decomposed rock.

13.1.10 Example Problem

The *t-z* method is illustrated by the solution of the problem shown in Figure 13.10. The *t-z* curves and the *q-w* curve are hypothetical but include nonlinear behavior for small movements of the pile and constant values of load transfer after a given amount of movement of the pile.

The example was solved by use of the computer. The first step was to assume a number of tip movements, starting with a small value and with increasing values, as shown in Table 13.4. The final tip movement was large enough to ensure the computation of the ultimate value of pile-head load.

The pile is subdivided into a number of increments, depending on its length and the variability of the soil. With the smallest tip movement, the end-bearing curve is assessed to obtain a tip load. The bottom increment of the pile is then selected. The computer interpolates a *t-z* curve for the mid-height of the bottom increment, employs the tip movement, and computes the load transfer in side resistance along the bottom increment. The axial load at the top of the bottom increment can now be computed. The loads at the bottom and top of the bottom increment, the elastic shortening can now be computed for the bottom increment.

The assumption is made that the movement is linear over the bottom increment and a new midpoint movement can be obtained. The new mid-point movement is now used to obtain a new value of load transfer from the interpolated *t-z* curve. The procedure is continued until convergence is achieved for the bottom increment, where the load-transfer from the present solution and the just previous one is within the tolerance set by the user. The next increment above the bottom increment is then selected and solutions are made, increment by increment, up the length of the pile. The next value of tip load is selected and the procedure is repeated.

The output of the program may be tabulated or presented graphically. For the example problem, curves showing distribution of load with depth are given

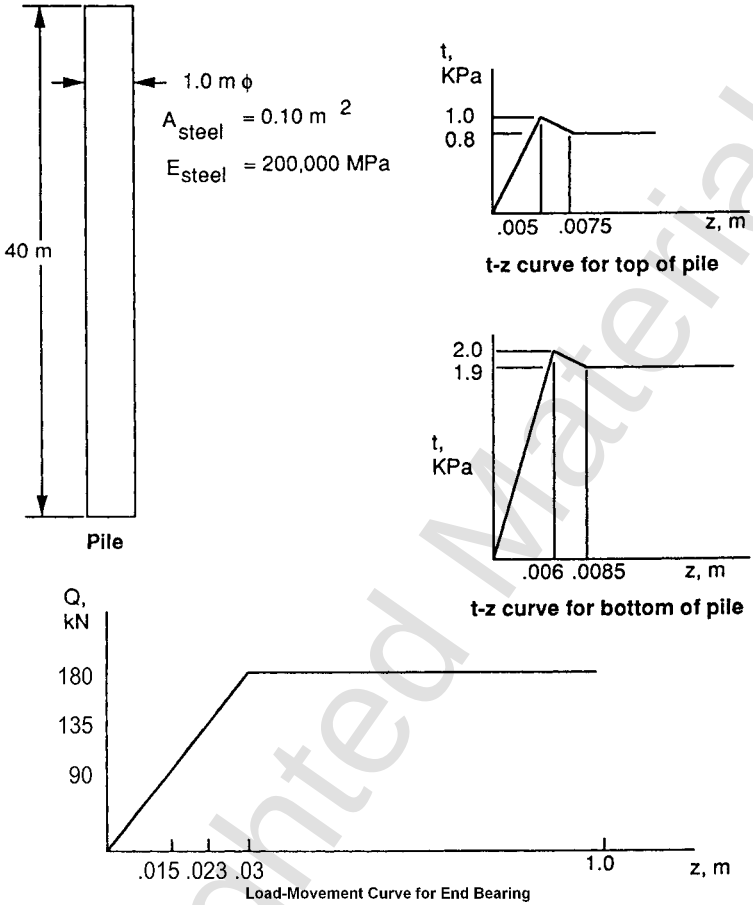

Figure 13.10 Pile properties and soil data for example problem.

TABLE 13.4 Summary of Load vs. Settlement Data at Pile Top and Pile Tip

Top Load KN.	Top Movement M.	Tip Movement M.	Tip Load KN.
0.4005E+02	0.1049E−02	0.1000E−02	0.6000E+01
0.8010E+02	0.2097E−02	0.2000E−02	0.1200E+02
0.1202E+03	0.3146E−02	0.3000E−02	0.1800E+02
0.1602E+03	0.4194E−02	0.4000E−02	0.2400E+02
0.2187E+03	0.8290E−02	0.8000E−02	0.4800E+02
0.2596E+03	0.1537E−01	0.1500E−01	0.9000E+02
0.3496E+03	0.3055E−01	0.3000E−01	0.1800E+03

in Figure 13.11 and a curve of the load versus settlement of the pile head is shown in Fig. 13.12. The numerical tabulation of output for points along the length of the pile is not shown but the engineer may consult the graphical and tabulated results to learn the stress and pile movement at any point along its length.

Partial Solution of Example Problem by Hand Computations A solution of the example was made by hand with an assumed tip movement of 0.0150 m. Only two increments of 20 m each were used along the pile. The curve in Figure 13.10 was consulted to find a tip load Q_b of 90 kN. With the assumption that the movement at the mid-height of the bottom increment was 0.015 m, Figure 13.13 was used to find the unit load transfer in side resistance of 1.625 kPa. The load in side resistance was then computed for the bottom increment.

$$Q_{s1} = (1.625)(\pi)(1)(20) = 102 \text{ kN}$$

The load at the top of the increment was 90 + 102 = 192 kN. The elastic shortening over the bottom increment may now be computed.

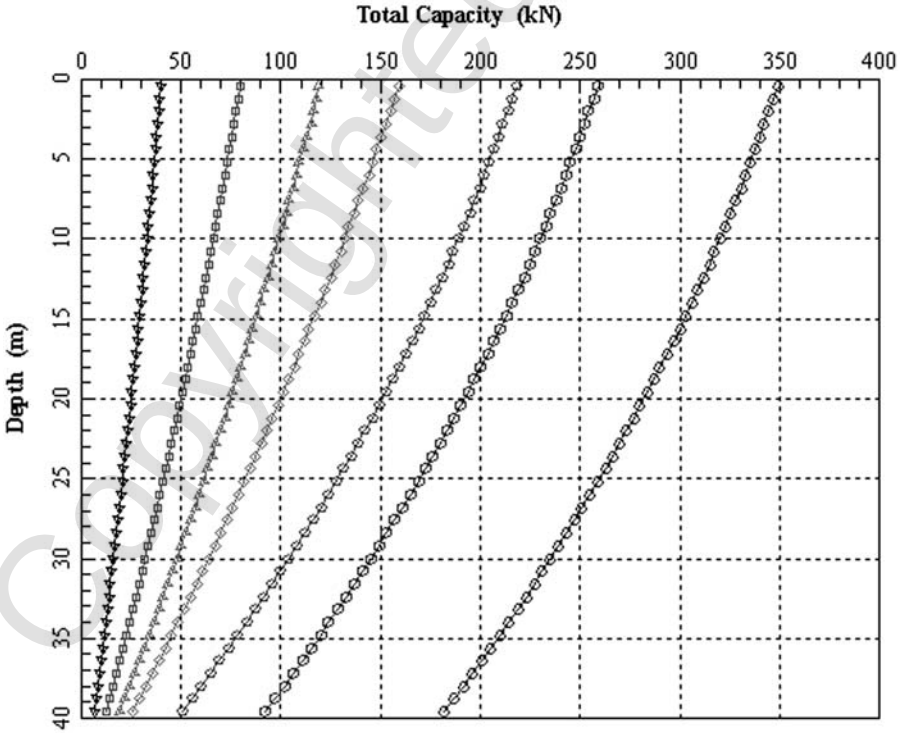

Figure 13.11 Load distribution curve for example problem.

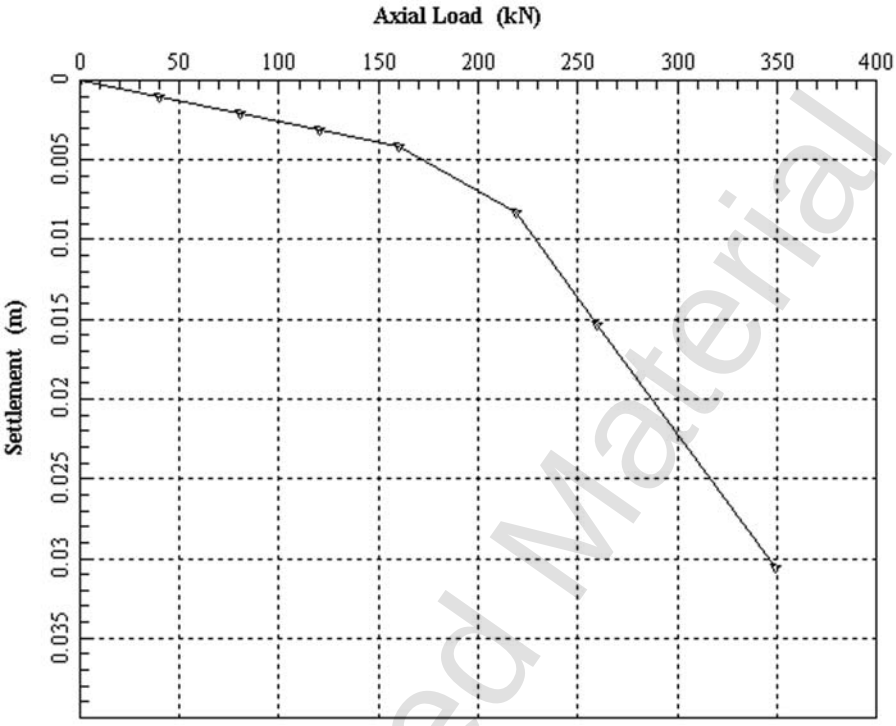

Figure 13.12 Load-settlement curve at pile head for example problem.

$$\delta_1 = \left(\frac{90 + 192}{2}\right)\left(\frac{20}{2x10^7}\right) = 0.0001410m$$

The movement at the top of the bottom increment may now be computed.

$$z_{\text{top}_1} = 0.0150 + 0.0001410 = 0.0151410m$$

Linear movement along the length of the bottom increment and the movement at the midpoint of the bottom increment are found.

$$z_{\text{mid}_1} = \left(\frac{0.0150 + 0.0151410}{2}\right) = 0.0150705m$$

The *t-z* curve for the bottom increment may now be consulted and the value of the load transfer is unchanged and no adjustment is needed in the computation.

The second increment is now considered and the movement at the top of the first increment may be used to obtain an estimate of the movement of the mid-height of the second increment, yielding a value of 1.075 kPa from Figure

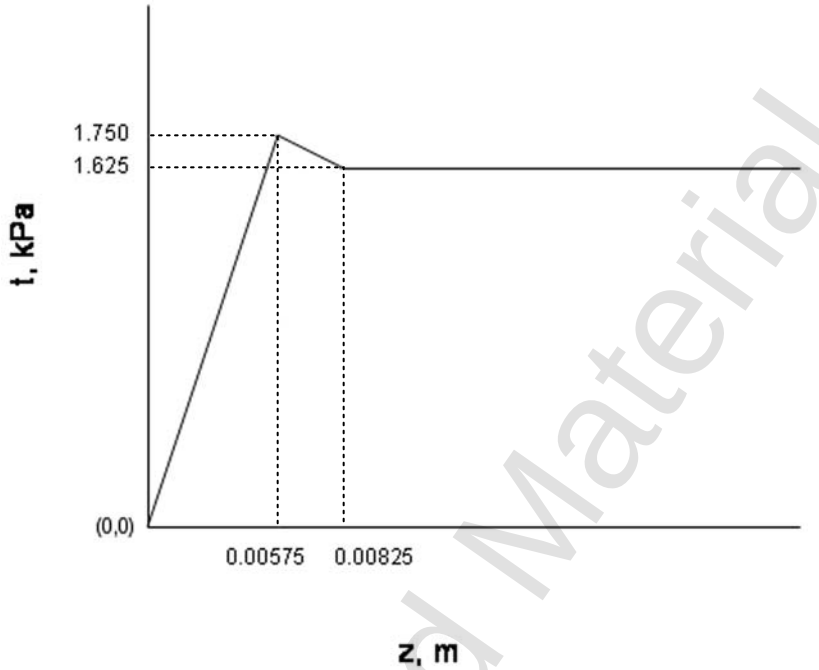

Figure 13.13 Interpolated t-z curve for 10 m above bottom of pile.

13.14. The load in side resistance of the second increment may now be computed.

$$Q_{s2} = (1.075)(\pi)(1)(20) = 67.5kN$$

The load at the top of the pile is 192 + 67.5 = 259.5. The elastic shortening of the top increment may now be computed.

$$\delta_2 = \left(\frac{192 + 259.5}{2}\right)\left(\frac{20}{2x10^7}\right) = 0.000226m$$

The movement at the top of the pile may now be computed.

$$z_{\text{top}_2} = 0.0151410 + 0.000226 = 0.015367m$$

The midpoint movement of the top increment may now be computed.

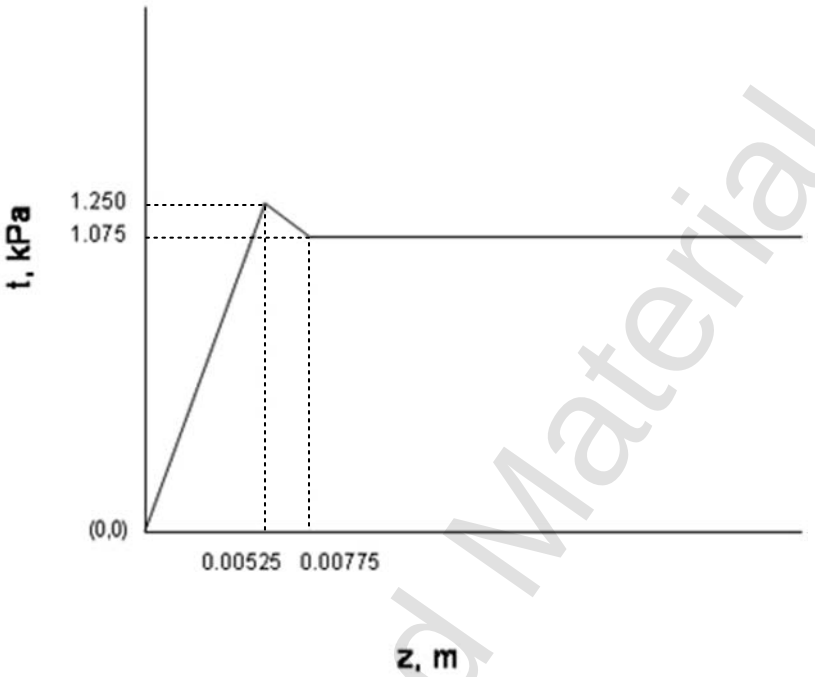

Figure 13.14 Interpolated t-z curve for 30 m above bottom of pile.

$$z_{\text{mid}_2} = \left(\frac{0.0151410 + 0.015367}{2}\right) = 0.0152540m$$

The *t-z* curve for the top increment may now be consulted and the value of load transfer is unchanged and no adjustment is needed in the computation.

The results for the hand solution and for the computer solution may now be shown.

	Load at top of pile, kN	Movement at top of pile, m
Hand	259.5	0.015367
Computer	259.6	0.01537

The hand solution and the computer solution yielded almost exact results because the pile was relatively stiff and because the computed mid-point movements did not change the load transfer values in side resistance from the values initially assumed. However, the hand computations shown above serve to illustrate the method of computation used in the *t-z* method of analysis.

13.1.11 Experimental Techniques for Obtaining Load-Transfer Versus Movement Curves

With the completion of a field load test on an instrumented pile, curves such as shown in Figs. 13.15a and 13.15b should be available. Figure 13.15a shows a load-settlement curve for the top of the pile. This curve may be obtained

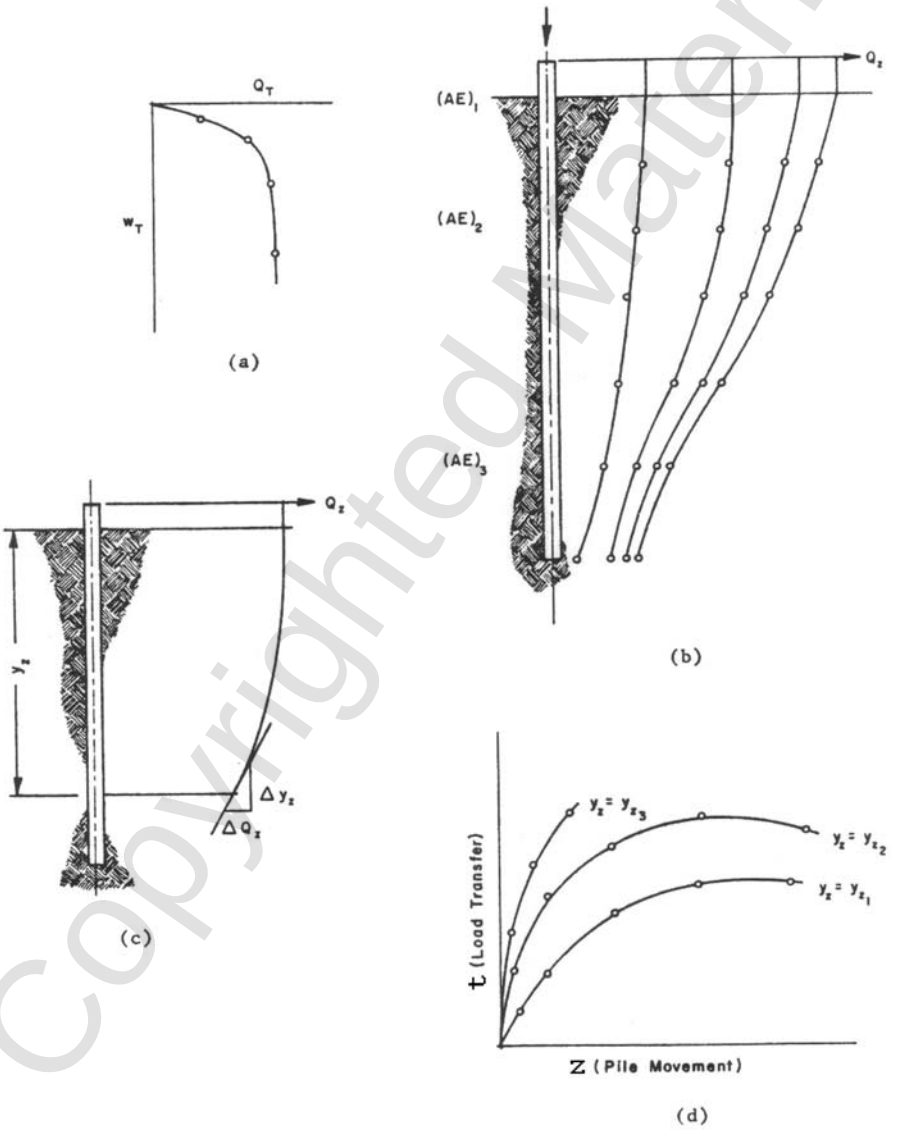

Figure 13.15 Development of load transfer versus movement of curves.

by measuring the load with a load cell and the downward movement of the top of the shaft with dial gauges. Figure 13.15b shows a set of curves which gives load in the pile at various points along its length for each of the applied loads. These data are obtained from instrumentation for measuring internal load in the pile at points along its length. Figures 13.15a and 13.15b indicate that four loads were applied to the pile; however, in the general case, several more loads would have been applied.

From the data in Figs. 13.15a and 13.15b, it is desired to produce a set of load-transfer curves such as are shown in Fig. 13.15d. Such curves can be produced for any desired depth. Figure 13.15c illustrates the procedure for obtaining a point on one of the curves. In this instance, the procedure is illustrated for obtaining load transfer at a depth y_z below the ground surface. For a particular load-distribution curve, corresponding to a particular load Q_z, the slope of the load-distribution curve is obtained at point y_z. In Fig. 13.15c this slope is indicated as the quantity $\Delta Q_z/\Delta y_z$. To obtain the load transfer t, the quantity is then divided by the pile circumference at the point y_z. Thus, the load transfer t will have the units of force per square of length.

The downward movement of the pile corresponding to the computed load transfer may be obtained as follows: (1) the settlement corresponding to the particular load in question is obtained from the curve in Fig. 13.15a; (2) the shortening of the pile is computed by dividing the cross-hatched area, shown in Fig. 13.15b, by the pile cross-sectional area times an effective modulus of elasticity; and (3) the downward movement of the pile at Point y_z is then computed by subtracting the shortening of the pile from the observed settlement.

The procedure enables one point on one load-transfer curve to be obtained for a particular depth. Other points may be obtained for the given depth by using the same procedures for other load-distribution curves. Other depths may be selected and a family of load-transfer curves may be obtained as shown in Fig. 13.15d. The settlement for a load-transfer curve for end bearing at the pile tip may be obtained as described above. The unit end bearing may be obtained by dividing the tip load by the area of the tip of the pile. As can be readily understood, accurate load-settlement and load-distribution data are required.

13.2 DESIGN FOR VERTICAL GROUND MOVEMENTS DUE TO DOWNDRAG OR EXPANSIVE UPLIFT

Any vertical movement of soil will affect the performance of a deep foundation. The problem of downdrag occurs when the direction of the soil movement is down relative to the foundation. The problem of uplift occurs when the direction of soil movement is up.

Peck et al. (1974) state: ''Several examples of unexpected settlement of large magnitude have been attributed to neglect of negative skin friction.''

Other failures have occurred when structures were founded on drilled shafts in expansive clay that swelled significantly after the shafts were constructed.

Tomlinson (1980) addressed the difficulty facing design engineers in designing for downdrag, stating: ''The calculation of the total negative skin friction or downdrag force on a pile is a matter of great complexity, and the time factor is of importance.'' This statement applies equally well to the case of drilled shafts in expansive soil. To solve these problems, the design engineer must know the axial load–transfer relationship, as well as the distribution of these movements versus depth and how these movements may vary with time.

13.2.1 Downward Movement Due to Downdrag

Loading by downdrag occurs when a shaft penetrates through a compressible layer that settles after the shaft is installed. The net effect of the downdrag is to increase the magnitude of axial loading in the shaft in the zone moving downward around the shaft. The severity of this problem depends on the interaction of the skin friction in the settling soil, the type of soil layering, and the characteristics of the bearing strata. Each case should be examined individually.

An example of loading by downdrag is shown in Figure 13.16. In this case, the soil profile consists of two layers of compressible soft clay, with an upper layer of sand between the layers of soft clay and a lower layer of sand providing end-bearing support for the shaft. The presence of two compressible layers of clay permits the upper sand layer to move downward around the pile. This situation may not be recognized because downdrag is mistakenly thought to occur only in layers of clay. One should recognize that downdrag could occur in any type of soil that moves downward around the shaft.

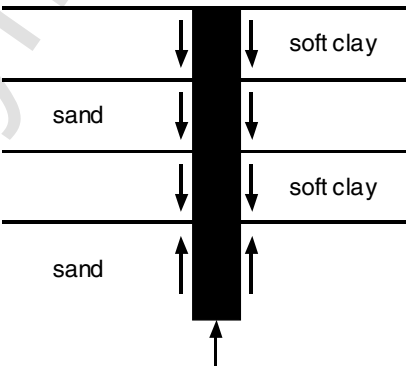

Figure 13.16 Soil profile susceptible to loading by downdrag.

The design of drilled shafts that are subjected to downdrag requires an analysis of the vertical settlement of soil versus depth. The methods of (EM) 1110-1-1904 Settlement Analysis may be used to estimate the vertical soil movements.

A simplified illustration of the mechanics of downdrag is shown in Figure 13.17. The relative movement of the soil to the shaft in shown in Parts (a) and (b) of this figure. The effect of the downward-moving soil is shown in Part (c). This effect increases the axial load in the drilled shaft above that applied at the top to the maximum value, Q_{max}, at an intermediate point along the depth of the shaft.

13.2.2 Upward Movement Due to Expansive Uplift

Swelling soils are found throughout the United States. The severity of problems due to swelling soils depends on the variation of the moisture content of the soil from dry to wet conditions. In general, the worst problems are found in areas with highly expansive clays where the amount of rainfall varies widely from year to year. In arid areas, problems are minimized because access to water is limited and the soils usually remain dry. In areas with high rainfall, problems are minimized because the wet conditions allow the soils to remain fully swollen.

A good indicator of the shrink-swell potential of the soil is the plasticity index. Plasticity index values above 35 are usually associated with clays with high swell potential. However, some highly plastic soils may be nonexpansive. Soils with plasticity index values less than 25 are generally considered to

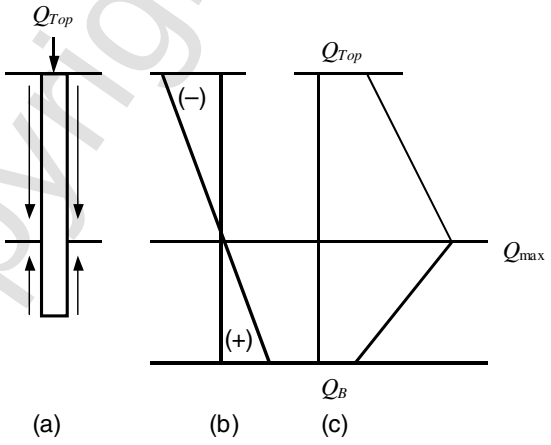

Figure 13.17 Mechanics of downdrag: (a) example problem; (b) relative movement of a drilled shaft relative to soil; (c) distribution of axial load along a drilled shaft.

have low swell potential, and soils with values between 25 and 35 are considered to have marginal swell potential.

PROBLEMS

P13.1. The computer program that solves a problem by use of the *t-z* method makes use of difference equations, where the difference between successive values of axial displacement of a pile is employed in the computer solution. What two sources of computational error can occur and what steps can the engineer take to minimize the errors?

P13.2. Your design is heavily dependent on the accuracy of the load-transfer curves shown in Figs. 13.3 and 13.4. What options do you have if you wish to validate the values shown in the curves?

P13.3. Present your ideas of why the curve in Fig. 13.7 for bored piles in cohesionless soil shows increased values of end bearing with increased settlement.

P13.4. (a) Re-work the hand computations in the example by keeping all of the input the same except that the thickness of the wall of the pile is 20 mm. (b) Plot curves showing distribution of load along the length of the pile using results from the computer and from the hand computations. Explain the differences in the curves. (c) Make a numerical comparison of the elastic shortening of the pile for the three solutions. (d) How would the solution differ if the pile had a nonlinear *AE* curve along its length?

P13.5. The calcareous soil at the Northwest Shelf in the ocean off the coast of Australia is strain-softening to a severe extent. What technique could be used to ensure that long piles supporting offshore platforms do not plunge under axial loading?